JCI The Journal of Clinical Investigation

Inactivation of paracellular cation-selective claudin-2 channels attenuates immune-mediated experimental colitis in mice

Preeti Raju, … , Sachiko Tsukita, Jerrold R. Turner

J Clin Invest. 2020. https://doi.org/10.1172/JCI138697.

Research In-Press Preview Cell biology Gastroenterology

Graphical abstract

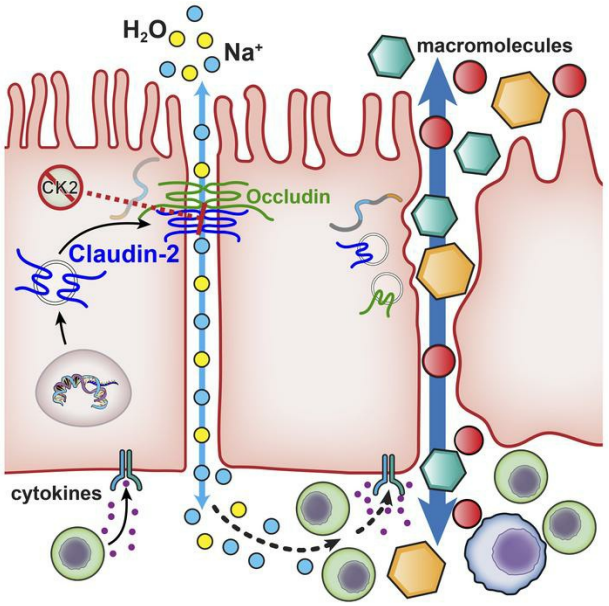

Inactivation of paracellular cation-selective claudin-2 channels attenuates immune-mediated experimental colitis in mice

Preeti Raju,[1] Nitesh Shashikanth,[1] Pei-Yun Tsai,[2] Pawin Pongkorpsakol,[1] Sandra Chanez-Parades,[1] Peter R. Steinhagen,[1] Wei-Ting Kuo,[1] Gurminder Singh,[1,2] Sachiko Tsukita,[3] and Jerrold R. Turner[1,2]

[1] Laboratory of Mucosal Barrier Pathobiology, Department of Pathology, Brigham and Women's Hospital and Harvard Medical School, Boston, MA, USA

[2] Department of Pathology, The University of Chicago, Chicago, Illinois, USA

[3] Laboratory of Biological Science, Graduate School of Frontier Biosciences and Graduate School of Medicine, Osaka University, Osaka, Japan

Running header: Claudin-2-mediated flux promotes colitis

Authorship note: PR and NS contributed equally to this work and are listed alphabetically.

Conflict of interest: JRT is a co-founder of and shareholder in Thelium Therapeutics.

Word count: 9,446 (including references, methods, and figure legends)

Address correspondence to: Jerrold R. Turner, Brigham and Women's Hospital, Harvard Medical School, 77 Avenue Louis Pasteur, HNRB 730B, Boston, Massachusetts, USA. Phone: 617.525.8165; Email: jrturner@bwh.harvard.edu.

Abstract (200 words)

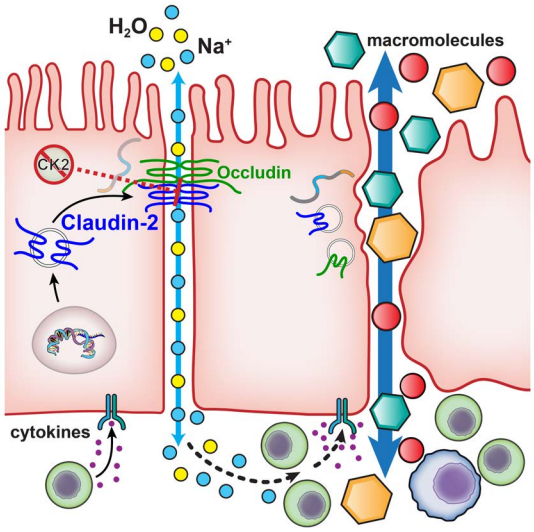

The tight junction protein claudin-2 is upregulated in disease. Although many studies have linked intestinal barrier loss to local and systemic disease, these have relied on macromolecular probes. In vitro analyses show however that these probes cannot be accommodated by size- and charge-selective claudin-2 channels. We sought to define the impact of claudin-2 channels on disease. Transgenic claudin-2 overexpression or IL-13-induced claudin-2 upregulation increased intestinal small cation permeability in vivo. IL-13 did not however affect permeability in claudin-2-knockout mice. Claudin-2 is therefore necessary and sufficient to effect size- and charge-selective permeability increases in vivo. In chronic disease, T-cell transfer colitis severity was augmented or diminished in claudin-2 transgenic or knockout mice, respectively. We translated in vitro data suggesting that casein kinase-2 (CK2) inhibition blocks claudin-2 channel function and found that CK2 inhibition prevented IL-13-induced, claudin-2-mediated permeability increases in vivo. In chronic immune-mediated colitis, CK2 inhibition attenuated progression in claudin-2-sufficient, but not claudin-2-knockout, mice, i.e., the effect was claudin-2-dependent. Paracellular flux mediated by claudin-2 channels can therefore promote immune-mediated colitis progression. Although the mechanisms by which claudin-2 channels intensify disease remain to be defined, these data suggest that claudin-2 may be an accessible target in immune-mediated disorders, including inflammatory bowel disease.

Brief Summary

This study shows that claudin-2 upregulation, which enhances paracellular flux of cations and water, but not larger molecules, promotes immune-mediated colitis progression and can be targeted therapeutically.

Introduction

Barriers that define distinct tissue compartments and separate self from non-self are necessary for survival of multicellular organisms. In some organs, for example the integument and bladder, the barrier is nearly impermeant to water, ions, and macromolecules. Other sites, however, including the intestine and renal tubules, require selectively permeable barriers (1-4). Both selective permeability and barrier function are defined by the epithelial tight junction (5, 6).

Paracellular permeability reflects the sum of separate tight junction pore and leak pathways. The pore pathway is a high-capacity, size- and charge-selective route whose permeability is primarily defined by the subset of claudin family proteins expressed (7-9). In contrast, the low-capacity, charge-nonselective leak pathway is permeable to macromolecules with diameters up to ~125 Å. Nearly all studies of in vivo intestinal barrier function have relied on large probes, e.g., 4 kD FITC-dextran (28 Å diameter), that can cross the leak pathway but are excluded by the ~8 Å maximum diameter pore pathway.

Claudin-2, a prototypic pore-forming claudin, forms actively-gated channels that are selective for water and small cations (10-14). Despite forming a high-capacity cation and water channel in vitro (11, 12, 15, 16), claudin-2 function has been difficult to define in vivo. Although claudin-2 is expressed in epithelial cells lining the small intestine, colon, pancreatobiliary tree, renal tubules, and, possibly, seminiferous tubules (17-20), claudin-2 knockout induces subtle phenotypic changes that are only apparent under stress (3, 21, 22). This may, in part, reflect some functional redundancy between claudin-2 and claudin-15, which also forms paracellular channels that are selective for small cations and water (10, 13, 16, 22-24).

Within the intestinal epithelium, claudin-2 is highly expressed at birth but rapidly downregulated, in concert with claudin-15 upregulation, at the time of weaning in rodents and humans (22, 25, 26). Intestinal epithelial claudin-2 expression is reactivated in inflammatory states including celiac disease (26-28), infectious enterocolitis (29), and inflammatory bowel disease (IBD), where the degree of upregulation correlates directly with disease severity (30-32). Although previous studies have shown that preservation of the leak pathway barrier to macromolecular flux, e.g., by myosin light chain kinase inhibition, limits both claudin-2 upregulation and immune-mediated colitis severity (33-39), contributions of the pore pathway to

disease development have not been studied. Nevertheless, many have hypothesized that claudin-2 upregulation contributes to tissue injury and promotes disease progression (27, 30, 40).

The impact of claudin-2 upregulation in disease has been studied in *C. rodentium* infectious colitis (29) and chemical (DSS) colitis models (41, 42) using claudin-2 transgenic ($Cldn2^{Tg}$) and knockout ($Cldn2^{-/-}$)[§] mice. In both cases claudin-2 knockout augmented disease severity while claudin-2 overexpression was protective. This contrasts sharply with the effects of increased leak pathway permeability and suggests that claudin-2-mediated pore pathway flux may be an adaptive response that promotes mucosal repair and homeostasis. Claudin-2 function has not, however, been studied in the context of immune-mediated, experimental colitis, thereby leaving the question of how claudin-2 upregulation might impact human disease unanswered.

Here, we assessed the effects of intestinal epithelial claudin-2 overexpression or knockout on in vivo pore pathway permeability and progression of immune-mediated, experimental IBD. Claudin-2 upregulation was required for cytokine-induced pore pathway permeability increases. Immune-mediated colitis severity was intensified in $Cldn2^{Tg}$ $Rag1^{-/-}$ mice but attenuated by either genetic claudin-2 deletion or pharmacological claudin-2 channel inactivation. These data illuminate the differences between distinct forms of paracellular flux and indicate that discrimination between pore and leak pathway regulation is critical to advancing our understanding of disease-associated barrier loss. The data also provide insight into the impact of claudin-2 expression in human diseases, including IBD, and the therapeutic potential of claudin-2 channel inhibition.

[§] Although *Cldn2* is X-linked, for simplicity male and female mice are both referred to as $Cldn2^{+/+}$ *or* $Cldn2^{-/-}$. All studies reported here were performed in both sexes and yielded similar results.

Results

Claudin-2 expression is necessary and sufficient for IL-13-induced barrier loss in vivo

We and others have shown that intestinal epithelial claudin-2 expression, which is limited in adults, can be upregulated in response to IL-13 in vitro and in vivo (26, 30, 31, 43). This IL-13-induced claudin-2 expression enhances pore pathway permeability of cultured monolayers in vitro (26, 30, 31, 43). To define the impact of IL-13 and contributions of claudin-2 on paracellular permeability in vivo, we analyzed intestinal tissues from wild type (*Cldn2*$^{+/+}$) and *Cldn2*$^{-/-}$ mice. Neither IL-13 treatment nor claudin-2 knockout affected colonic histopathology (Figure 1A). As expected, IL-13 markedly increased claudin-2 expression within colonic crypt epithelia of wild type, but not *Cldn2*$^{-/-}$ mice (Figure 1B). Quantitative analysis showed that claudin-2 expression in IL-13-treated mice was 1.9-fold that of vehicle treated mice (Figure 1C, D). In contrast, expression of other tight junction proteins was unaffected by IL-13 treatment (Figure 1C, D).

Claudin-2 expression, whether induced genetically or by cytokines, specifically enhances flux across the charge- and size-selective pore pathway but not the less selective leak pathway in vitro (14, 15, 43-46). To define the impact of IL-13-induced claudin-2 upregulation in vivo, bi-ionic potentials were measured to determine paracellular permeability of Na^+ and larger monovalent cations (14, 45, 47). IL-13 increased paracellular permeability of Na^+, methylamine, and, to a lesser extent, ethylamine, but not the larger cations tetramethylammonium, tetraethylammonium, or N-methyl-D-glucamine (Figure 1E). This size-selective permeability increase is characteristic of claudin-2 channel activity (14-16, 48-50), but does not exclude the possibility that other cation-selective pore-forming claudins, e.g., claudin-15 (10, 13, 22), contribute to IL-13-induced barrier loss in vivo. We therefore asked if claudin-2 was required for IL-13-induced barrier loss. Prior to IL-13 treatment, paracellular permeability was similar in wild type and *Cldn2*$^{-/-}$ mice, consistent with limited claudin-2 expression in adults. IL-13 treatment was not, however, able to increase paracellular permeability of small cations, including Na^+ and methylamine in *Cldn2*$^{-/-}$ mice (Figure 1F). Claudin-2 is therefore necessary for IL-13-induced increases in intestinal pore pathway permeability.

In order to determine if claudin-2 upregulation is sufficient to mediate the effects of IL-13 on intestinal cation permeability, transgenic mice expressing EGFP-tagged mouse claudin-2 from the intestinal epithelial-specific *Vil1* promoter (*Cldn2*^{Tg}) were characterized (29). Total

claudin-2 expression (the sum of endogenous and EGFP-claudin-2) in these *Cldn2*^{Tg} mice was similar in distribution (Figure 1G) to that of IL-13-treated wild type mice (Figure 1B) and increased 3.3-fold relative to *Cldn2*$^{+/+}$ mice that did not receive IL-13 (Figure 1H, I). Moreover, transgenic EGFP-claudin-2 expression increased paracellular permeability of Na^+, methylamine, and, to a lesser extent, ethylamine, but not larger cations, in a manner that recapitulated the effect of IL-13 on wild type mice (Figure 1J). Claudin-2 is, therefore, both necessary and sufficient to mediate IL-13-induced barrier loss in vivo.

Transgenic claudin-2 expression exacerbates immune-mediated colitis

We have found that severity and duration of infectious colitis are reduced in these EGFP-*Cldn2*^{Tg} mice (29). A study of similar transgenic mice expressing human claudin-2 from the same *Vil1* promoter demonstrated that claudin-2 overexpression was also protective in DSS-induced, chemical colitis (41). Conversely, claudin-2 knockout exacerbated infectious and chemical colitis (29, 42). These data suggest that claudin-2-mediated pore pathway permeability increases may be adaptive, i.e., beneficial in IBD. To test this hypothesis, we compared severity of experimental IBD in immunodeficient *Cldn2*^{Tg} *Rag1*$^{-/-}$ and *Cldn2*$^{+/+}$ *Rag1*$^{-/-}$ mice using the well-established T cell transfer model (33, 51).

Disease was significantly more severe in *Cldn2*^{Tg} *Rag1*$^{-/-}$ mice relative to *Cldn2*$^{+/+}$ *Rag1*$^{-/-}$ mice. This was demonstrated by more extensive weight loss (Figure 2A) and greater disease activity (Figure 2B). Consistent with increased disease severity, leak (macromolecular) and unrestricted (epithelial damage) pathway permeabilities, measured as 4kD dextran flux, were also markedly greater in *Cldn2*^{Tg} *Rag1*$^{-/-}$ mice relative to *Cldn2*$^{+/+}$ *Rag1*$^{-/-}$ mice (Figure 2C) (29). Colitis increased claudin-2 expression in *Cldn2*$^{+/+}$ *Rag1*$^{-/-}$ and *Cldn2*^{Tg} *Rag1*$^{-/-}$ mice (Figure 2D). In colitic *Cldn2*$^{+/+}$ *Rag1*$^{-/-}$ mice, the region of claudin-2 expression extended beyond crypt bases to include the entire lower half of elongated crypts, i.e., the transit amplifying zone. The region of endogenous claudin-2 expression was similarly increased in colitic *Cldn2*^{Tg} *Rag1*$^{-/-}$ mice, but these mice also expressed transgenic, EGFP-claudin-2 in the upper half of the crypt and surface epithelium (Figure 2D). It is possible that this expanded area of claudin-2 expression contributed to earlier increases in fecal water content in *Cldn2*^{Tg} *Rag1*$^{-/-}$, relative to *Cldn2*$^{+/+}$ *Rag1*$^{-/-}$, mice (Figure 2E).

Consistent with more weight loss and higher disease activity scores, mucosal IFNγ

(Figure 2F) and TNF (Figure 2G), T cell recruitment (Figure 2H), and overall histopathology (Figure 2I) were greater in *Cldn2*^{Tg} *Rag1*$^{-/-}$ mice relative to *Cldn2*$^{+/+}$ *Rag1*$^{-/-}$ mice. Thus, in contrast to infectious and chemical colitis, intestinal epithelial claudin-2 overexpression accelerates onset and enhances severity of experimental IBD, i.e., chronic immune-mediated colitis.

Claudin-2 deficiency limits progression of immune-mediated colitis

The increased severity of immune-mediated disease in *Cldn2*^{Tg} *Rag1*$^{-/-}$ mice was unexpected. We therefore assessed the impact of claudin-2 knockout on immune-mediated experimental colitis. Disease onset, as defined by weight loss (Figure 3A) and disease activity (Figure 3B) was markedly delayed in *Cldn2*$^{-/-}$ *Rag1*$^{-/-}$ mice, which were also largely protected from increases in leak pathway permeability (Figure 3C). T cell transfer increased claudin-2 expression in *Cldn2*$^{+/+}$ *Rag1*$^{-/-}$ but not *Cldn2*$^{-/-}$ *Rag1*$^{-/-}$ mice (Figure 3D), and fecal water increases were delayed in the absence of claudin-2 (Figure 3E). Finally, mucosal cytokine production (Figure 3F, G), T cell recruitment (Figure 3H), and histopathology (Figure 3I) were markedly reduced in *Cldn2*$^{-/-}$ *Rag1*$^{-/-}$ mice. Genetic claudin-2 inhibition therefore reduces disease progression, suggesting that claudin-2 may be a viable therapeutic target.

Despite reduced disease severity, mortality is increased by claudin-2 deficiency

Unexpectedly, T cell transfer caused much greater mortality in *Cldn2*$^{-/-}$*Rag1*$^{-/-}$ mice relative to *Cldn2*$^{+/+}$ *Rag1*$^{-/-}$ mice (Figure 4A). The manner of progression to death was, however, atypical. In contrast to *Cldn2*$^{+/+}$ *Rag1*$^{-/-}$ mice, which died following progressive disease, *Cldn2*$^{-/-}$ *Rag1*$^{-/-}$ mice were typically well until ~6 weeks after T cell transfer, at which time a subset became inactive and hunched, despite limited weight loss, and died within days. The distinct pattern of disease prior to death of *Cldn2*$^{-/-}$ *Rag1*$^{-/-}$ mice was explained upon necropsy. Gross intestinal obstruction (Figure 4B) with ischemic injury superimposed on experimental IBD (Figure 4C) was present in 50% of *Cldn2*$^{-/-}$ *Rag1*$^{-/-}$ mice that died. In contrast, intestinal obstruction was not present in any *Cldn2*$^{+/+}$ *Rag1*$^{-/-}$ mice. Thus, even though it reduced colitis severity, claudin-2 knockout promoted obstruction that compromised overall survival.

Fibrostenosing strictures commonly cause intestinal obstruction in Crohn's disease. Picrosirius red stains (Figure 4D) were used to assess fibrosis in colons from *Cldn2*$^{-/-}$ *Rag1*$^{-/-}$ and

Cldn2$^{+/+}$ *Rag1*$^{-/-}$ mice; only minimal fibrosis was detected (Figure 4E). Fibrosis cannot, therefore, explain intestinal obstruction in *Cldn2*$^{-/-}$ *Rag1*$^{-/-}$ mice. We also considered dysmotility as a potential cause of obstruction. No differences in small intestinal (Figure 4F) or colonic (Figure 4G) motility were, however, detected between *Cldn2*^{Tg}, *Cldn2*$^{+/+}$, and *Cldn2*$^{-/-}$ mice. The intestinal obstruction observed in *Cldn2*$^{-/-}$ *Rag1*$^{-/-}$ mice is not, therefore, secondary to fibrosis or dysmotility.

Insufficient fecal hydration leads to increased mortality of *Cldn2*$^{-/-}$ *Rag1*$^{-/-}$ mice

Having excluded motility and structural alterations of the bowel wall, we considered the possibility that insufficient luminal hydration could lead to obstruction in *Cldn2*$^{-/-}$ *Rag1*$^{-/-}$ mice. Although fecal water increased during experimental IBD progression in *Cldn2*$^{-/-}$ *Rag1*$^{-/-}$ mice, it was markedly attenuated relative to *Cldn2*$^{+/+}$ *Rag1*$^{-/-}$ mice (Figure 3E). In contrast, fecal Na^+ did not increase during experimental IBD in *Cldn2*$^{-/-}$ *Rag1*$^{-/-}$ (Figure 5A). To better understand this difference, we assessed expression of the two claudins, 2 and 15, that mediate paracellular Na^+ and water flux in the intestine as well as ZO-1 and occludin (Figure 5B). Strikingly, disease induced marked claudin-15 upregulation in *Cldn2*$^{-/-}$ *Rag1*$^{-/-}$, but not *Cldn2*$^{+/+}$ *Rag1*$^{-/-}$, mice (Figure 5B, C). Conceptually, claudin-15 upregulation could reflect an effort to compensate for the lack of claudin-2 (4, 22). Claudin-15 was not, however, able to complement claudin-2 knockout, as fecal Na^+ and water did not increase in *Cldn2*$^{-/-}$ *Rag1*$^{-/-}$ mice. This is surprising, as available data indicate that claudin-2 and claudin-15 are, at least in part, functionally redundant in vitro and in vivo (4, 13, 26, 52). Nevertheless, these data indicate that these closely-related claudins must have distinct biophysical properties (13) or mechanisms of pore regulation (50) that allow claudin-2, but not claudin-15, to increase fecal Na^+ and water during progression of colitis. Colonic epithelial occludin expression was slightly, but significantly, reduced in colitic *Cldn2*$^{+/+}$ *Rag1*$^{-/-}$ and *Cldn2*$^{-/-}$ *Rag1*$^{-/-}$ mice, relative to healthy controls, but there was no difference between genotypes (Figure 5C).

To determine if insufficient luminal hydration was responsible for obstruction and mortality in *Cldn2*$^{-/-}$ *Rag1*$^{-/-}$ mice, polyethylene glycol was added to the drinking water in order to induce mild osmotic diarrhea. This prevented the development of intestinal obstruction in *Cldn2*$^{-/-}$ *Rag1*$^{-/-}$ mice (Figure 5D). Polyethylene glycol treatment did not however affect claudin-15 expression (Figure 5E), suggesting that inadequate luminal hydration was not the stimulus for

this upregulation. Disease severity and histopathology scores were unaffected by polyethylene glycol (Figure 5F), but survival of *Cldn2*$^{-/-}$ *Rag1*$^{-/-}$ mice improved to equal that of *Cldn2*$^{+/+}$ *Rag1*$^{-/-}$ mice (Figure 5G). These data therefore demonstrate that claudin-2-mediated water efflux contributes significantly to diarrhea and that the resulting increases in luminal fluid prevent intestinal obstruction.

CK2 inhibition prevents claudin-2 function but does not affect DSS colitis

We have identified a series of molecular interactions between occludin, ZO-1, and claudin-2 that are regulated by casein kinase-2 (CK2) (50). CK2 normally phosphorylates S408 within the occludin C-terminal cytoplasmic tail, but CK2 inhibition allows dephosphorylation of this site (53). This enhances the affinity of occludin for the ZO-1 U5-GuK domain (50, 54). Binding of this bimolecular complex to the C-terminus of claudin-2 via the ZO-1 PDZ1 domain inactivates claudin-2 pore function (Figure 6A) (50). In vitro, CK2 inhibition reversed IL-13-induced, claudin-2-mediated permeability increases (50). To determine if this regulatory pathway is active in vivo, mice were treated with IL-13 with or without a CK2 inhibitor. IL-13 robustly induced claudin-2 upregulation, and this was not affected by the CK2 inhibitor (Figure 6B). CK2 inhibition was however sufficient to completely block IL-13-induced increases in intestinal paracellular cation permeability (Figure 6C). Thus, CK2 inhibition can inactivate claudin-2 channels in vivo.

The efficacy of CK2 inhibition in blocking claudin-2 pore function suggested that this might be an effective therapy for experimental IBD. Previous work has, however, shown that CK2 is upregulated in DSS colitis and IBD and defined CK2 as a critical regulator of epithelial survival, proliferation, and migration in chronic intestinal inflammation (55). We were, therefore, concerned that systemic CK2 inhibition could exacerbate colitis. To address this, CK2 was inhibited using CX4945, an orally-bioavailable CK2 inhibitor (56-59). CK2 inhibition neither accelerated nor attenuated DSS-induced weight loss (Figure 6D) but caused a slight reduction in histopathology (Figure 6E). The effects of CK2 inhibition were identical in *Cldn2*$^{+/+}$ and *Cldn2*$^{-/-}$ mice, indicating that they were independent of claudin-2 function. The data further indicate that CK2 is not essential to mucosal homeostasis and that CK2 inhibition may not have the in vivo toxicities predicted by previous in vitro studies.

CK2 inhibition attenuates immune-mediated, experimental IBD via a claudin-2-dependent mechanism

As in human IBD (55), intestinal epithelial CK2 expression increased during immune-mediated experimental colitis (Figure 7A). The magnitude of this upregulation was similar in *Cldn2*$^{-/-}$ *Rag1*$^{-/-}$ and *Cldn2*$^{+/+}$ *Rag1*$^{-/-}$ mice (Figure 7A). To assess the impact of CK2 upregulation, mice received a CK2 inhibitor by daily gavage. This treatment, which was not initiated until day 10 after T cell transfer, markedly reduced disease severity, as indicated by weight loss (Figure 7B) and disease activity scores (Figure 7C). This beneficial effect of CK2 inhibition was claudin-2-dependent, as the inhibitor was ineffective in *Cldn2*$^{-/-}$ *Rag1*$^{-/-}$ mice (Figure 7B). CK2 inhibition also limited increases in fecal water (Figure 7C) and Na^+ (Figure 7D) in *Cldn2*$^{+/+}$ *Rag1*$^{-/-}$ mice such that they were similar to *Cldn2*$^{-/-}$ *Rag1*$^{-/-}$ mice. This further suggests that CK2 inhibition reduced claudin-2 pore function in vivo. Importantly, despite causing the phenotype of *Cldn2*$^{+/+}$ *Rag1*$^{-/-}$ mice to mimic that of *Cldn2*$^{-/-}$ *Rag1*$^{-/-}$ mice, CK2 inhibition did not increase mortality of *Cldn2*$^{+/+}$ *Rag1*$^{-/-}$ mice (Figure 7E). CK2 inhibitor-induced claudin-2 channel inactivation was nevertheless sufficient to limit leak and unrestricted pathway barrier loss (Figure 7F), mucosal T cell infiltration (Figure 7G), and histopathologic progression (Figure 7H) in *Cldn2*$^{+/+}$ *Rag1*$^{-/-}$ mice to levels observed in *Cldn2*$^{-/-}$ *Rag1*$^{-/-}$ mice. Although CK2 is widely expressed and known to be promiscuous with respect to substrates, the absence of apparent toxicities suggests that CK2 does not serve other critical functions in the context of immune-mediated experimental colitis. The dependence on claudin-2 expression indicates however that CK2 inhibition limits disease by inactivating claudin-2 channels.

Discussion

In contrast to macromolecular barrier loss, no studies have characterized the impact of size- and charge-selective permeability increases on immune-mediated colitis. In vitro studies have shown that claudin-2, which is upregulated in colitis, creates paracellular channels that accommodate water and Na^+ but not larger molecules. Here, we focused on the effects of in vivo claudin-2 expression on barrier function and immune-mediated disease. Claudin-2 upregulation was required for IL-13-induced increases in paracellular water and Na^+ permeability; these changes were recapitulated by transgenic claudin-2 overexpression in vivo. We then sought to determine whether claudin-2 upregulation in immune-mediated experimental IBD represents an adaptive, pro-homeostatic response or, alternatively, enhances disease progression. The data indicate that claudin-2 upregulation promotes mucosal immune activation and increases experimental IBD severity. Conversely, we found that in vivo CK2 inhibition inactivates claudin-2 channels, prevents acute claudin-2-mediated paracellular permeability increases, and improves outcomes in experimental IBD.

Despite well-characterized size- and charge-selectivity in vitro (11, 12, 14, 15, 43, 46), the impact of claudin-2 expression on in vivo barrier function has been controversial (27, 40, 41, 60). In part, this debate reflects the coexistence of claudin-2 upregulation and increased macromolecular flux in colitis (27, 40). The idea that claudin-2 channels can accommodate macromolecules is also supported by a report that flux of 4kD dextran (28 Å diameter) was increased by transgenic human claudin-2 expression (41). In contrast, the transgenic mice described here displayed size- and charge-selective permeability increases (29). The difference between these two claudin-2 transgenic mice is puzzling, but cannot be due to the promoter used, as both studies relied on the same 9 kB *Vil1* promoter (61). One difference however was increased epithelial proliferation, in the absence of any stimuli, in human claudin-2 transgenic but not mouse claudin-2 transgenic mice (29, 41). This suggests that low grade epithelial damage may be present in human claudin-2 transgenic mice and that this explains the reported increase in 4kD dextran flux (41). Although it is possible that mouse claudin-2 function was modified by the N-terminal EGFP tag, this is unlikely based on previous in vitro and in vivo analyses (29, 50, 62, 63). The in vivo permeability changes induced by in vivo overexpression of EGFP-tagged mouse claudin-2 therefore mirror those of in vitro claudin-2 overexpression (12, 14, 15, 43).

Strikingly immune-mediated experimental IBD was far more severe in *Cldn2*^{Tg} *Rag1*$^{-/-}$

mice, while *Cldn2*$^{-/-}$ *Rag1*$^{-/-}$ mice were protected from colitis. This was unexpected given that reciprocal results, i.e., protection by claudin-2 overexpression and exacerbation by claudin-2 deletion, were observed in chemical and infectious colitis (29, 41, 42). Osmotically-induced diarrhea rescued *Cldn2*$^{-/-}$ mice from infectious colitis, indicating that claudin-2 promotes pathogen clearance by enhancing paracellular water efflux. Similarly, the fecal water increases induced by claudin-2 overexpression may dilute DSS within the distal colon to reduce mucosal injury in *Cldn2*^{Tg} mice. Thus, claudin-2-mediated water efflux may explain the protective effects of claudin-2 upregulation in both chemical and infectious colitis.

Consistent with claudin-2-mediated luminal water efflux, insufficient luminal hydration explains the increased mortality of *Cldn2*$^{-/-}$ *Rag1*$^{-/-}$ mice in immune-mediated experimental IBD. Moreover, this increased mortality was eliminated by osmotically-induced increases in luminal hydration. However, unlike infectious colitis, increased luminal hydration did not affect disease severity. This cannot, therefore, be the mechanism by which claudin-2 deletion reduces immune-mediated experimental IBD severity. One alternative explanation could be that claudin-2 expression increases, and claudin-2 knockout reduces, mucosal, i.e., lamina propria, Na^+ (22). This idea is supported by previous work showing that luminal Na^+, but not active transepithelial transport, is required to maintain villous lamina propria Na^+ concentrations of up to 900 mM, corresponding to osmolarities of up to 1,600 mOsm (64). Although villous lamina propria Na^+ concentrations have not been measured in claudin-2 or claudin-15 knockout mice, luminal Na^+ is reduced in these mice (22). Thus, claudin-2 deficiency could be expected to result in reduced luminal and villous lamina propria Na^+ concentrations in some situations. Together with previous work showing that increased Na^+ and hyperosmolarity activate salt-sensitive serum-glucocorticoid kinase 1 (SGK1) to enhance Th1 and Th17 cell differentiation (65-67), these data suggest the hypothesis that claudin-2 deficiency reduces, and claudin-2 overexpression enhances, lamina propria Na^+ to drive pathogenic T cell development. Consistent with this, a high salt diet is sufficient to increase mucosal Th17 cell frequency (66, 68) and to exacerbate DSS-induced chemical colitis (68, 69). Nevertheless, it remains unclear why claudin-15, which was upregulated in colitic *Cldn2*$^{-/-}$ *Rag1*$^{-/-}$ mice, was not sufficient to replace claudin-2 function and restore Th1 and Th17 cell differentiation. Further characterization of functional differences between claudin-2 and claudin-15 as well as their interactions with dietary Na^+ and effects on mucosal Na^+ is, therefore, warranted along with exploration of the impact of claudin-2

expression on tissue Na^+ concentrations and T cell differentiation.

We previously discovered a complex signaling pathway by which CK2 activity facilitates, and CK2 inhibition blocks, claudin-2 pore function (50). Although the responsible phosphatase has not been identified, in vitro analyses have shown that CK2 inhibition leads to occludin dephosphorylation at specific residues. Mutagenesis studies identified S408 within the occludin C-terminal tail as the key site which, when dephosphorylated, increases occludin affinity for the ZO-1 U5GuK domain. This bimolecular interaction increases anchoring, i.e. reduces fluorescent recovery after photobleaching (FRAP), of tight junction-associated occludin (50). Binding of this complex to claudin-2, via the ZO-1 PDZ1 domain, disrupts claudin-2 channel function. This can have profound functional consequences as, for example, CK2 inhibition is sufficient to acutely reverse claudin-2-mediated, IL-13-induced barrier loss in vitro (50).

Although CK2-dependent regulation of occludin S408 phosphorylation has not been confirmed in vivo, we previously used intravital imaging and FRAP of transgenic EGFP-occludin to demonstrate that CK2 inhibition increases occludin anchoring at the tight junction in vivo (50). Here, we have shown that the second part of this signal transduction mechanism, claudin-2 channel inactivation, also occurs in vivo. Importantly, the effect of CK2 inhibition was only apparent after claudin-2 upregulation and, characteristic of claudin-2 channels, was selective for Na^+ and methylamine cations.

To determine if pharmacological claudin-2 channel inactivation could be beneficial in chronic immune-mediated colitis, mice were dosed with a highly-specific, orally-bioavailable CK2 inhibitor that was well-tolerated in both preclinical studies and phase 1 clinical trials (70, 71). Consistent with claudin-2 channel inactivation, inhibitor treatment reduced fecal water and Na^+ increases during disease progression. This was claudin-2-dependent, as CK2 inhibition did not affect fecal water and Na^+ in *Cldn2*$^{-/-}$ *Rag1*$^{-/-}$ mice. Moreover, CK2 inhibition attenuated weight loss, T cell recruitment, and histopathology in *Cldn2*$^{+/+}$ *Rag1*$^{-/-}$ mice to levels seen in *Cldn2*$^{-/-}$ *Rag1*$^{-/-}$ mice. Again, this was claudin-2-dependent; CK2 inhibition did not benefit *Cldn2*$^{-/-}$ *Rag1*$^{-/-}$ mice. Thus, despite the promiscuity of CK2, the data indicate that the effects of CK2 inhibition are primarily due to claudin-2 channel inactivation. In contrast to claudin-2 knockout however, CK2 inhibition was not accompanied by intestinal obstruction or increases in mortality. This or similar approaches may therefore be safe for clinical use.

As a whole, our data indicate that epithelial claudin-2 upregulation promotes progression of immune-mediated experimental IBD. This contrasts sharply with infectious and chemical colitis, suggesting that claudin-2 pore function has pleiotropic effects on intestinal mucosal pathophysiology. The data also demonstrate that CK2 inhibition inactivates claudin-2 pores in vivo and, predominantly via this mechanism, limits colitis progression. Although the broad expression and multiple functions of CK2 may limit utility of CK2 inhibition in colitis, we anticipate that further molecular definition of claudin-2 channel function (14) will lead to development of more precisely-targeted therapies.

Methods

Mice

C57BL/6J mice (Stock# 000664) and *Rag1*$^{-/-}$ (B6.129S7-*Rag1*^{tm1Mom}/J) mice (Stock# 002216) were purchased from The Jackson Laboratory. Claudin-2 knockout mice on a C57BL/6J background have been described (4, 29). Transgenic EGFP-claudin-2 mice were generated using the 9kB villin promoter (29, 72). Mice were bred under specific pathogen-free conditions and used at 6 - 8 weeks of age. Littermates or co-housed mice were used for all experiments. Individual experiments were segregated, but all studies were performed in both sexes.

Cytokine and CK2 Inhibitor Treatment

Mice were injected i.p. with 1.0 to 2.5 μg (160 units) of recombinant murine IL-13 (R&D Systems) 14 hr prior to tissue harvest. Mice were injected i.p. with the CK2 inhibitor TBCA ((E)-3-(2,3,4,5-tetrabromophenyl)acrylic acid, 50 mg/kg; Sigma) 24 hours before and 2 hours after IL-13 injection. The CK2 inhibitor CX-4945 (kindly provided by Cylene Pharmaceuticals, San Diego, CA) was delivered by gavage twice daily at 75 mg/kg in DSS experiments. Because T cell transfer colitis experiments required treatment over much longer intervals, mice were gavaged only once each day, beginning 10 days after transfer. In an effort to compensate for the reduced treatment frequency, the drug dose was increased to 100 mg/kg,

Colitis induction

Acute colitis was induced by adding 3% DSS (Sigma) to drinking water and following mice over 8 days (35). Immune-mediated colitis was induced in immunodeficient *Rag1*$^{-/-}$ mice by transfer of $5x10^5$ purified $CD4^+CD45Rb^{hi}$ T cells, as described (33, 35). Disease activity was scored from 0 to 2 each for motor activity, fur texture, posture, and diarrhea (0–8), as described (33, 35).

Electrophysiology

Stripped proximal colonic mucosa was mounted in 0.3 cm^2 surface area Ussing chambers (Physiologic Instruments) containing 135 mM NaCl, 5 mM KOH, 1.3 mM $CaCl_2$, 0.4 mM $MgSO_4$, 0.3 mM NaH_2PO_4, 15 mM HEPES, 5.5 mM D-glucose, pH 7.4, and bubbled continuously with 100% O_2 at 37 °C. Resistance was calculated based on the potential generated by 10 μA square-wave pulses. NaCl dilution potentials were measured as reported previously

(43). Bi-ionic potentials were measured by replacing Na^+ (1.9 Å diameter) with methylamine (3.8 Å), ethylamine (4.6 Å), tetramethylammonium (5.6 Å), tetraethylammonium (6.6 Å), or N-methyl-D-glucamine (7.4 Å) as described (15, 50).

Intestinal Permeability, Motility, and Fecal Analyses

Mice were denied access to food but allowed water for 3 hr prior to gavage with 0.15 ml saline containing 12 mg fluorescein isothiocyanate-4 kD dextran (Sigma). Serum was collected 4 hours later and analyzed as described (34). Motility was determined using fluorescein isothiocyanate-70 kD dextran (73). Fecal Na^+ and water content were determined as described (29).

ELISA

Portions of colon (0.5 cm) were washed and homogenized in Bio-Plex buffers (Bio-Rad) as described (34). After freeze-thaw and sonication, supernatants (5 min at 4,500 x g) were analyzed for total protein using a Bradford assay (Bio-Rad) and cytokines using Ready-SET-Go! ELISA kits (eBioscience).

Antibodies

Mouse monoclonal anti-GFP, GFP-G1, Developmental Studies Hybridoma Bank, RRID AB_2619561; Rabbit polyclonal anti-claudin-2 (MH44), 51-6100, ThermoFisher, RRID AB_2533911; Rabbit polyclonal anti-claudin-2, HPA051548, Atlas Antibodies, RRID AB_2681530; Monoclonal mouse ant-claudin-2 (12H12), 32-5600, ThermoFisher, RRID AB_2533085; Rabbit monoclonal anti-claudin-4, ab210796, Abcam, RRID AB_2732879; Rabbit polyclonal anti-claudin-15, 38-9200, ThermoFisher, RRID AB_2533391; Rat monoclonal anti-occludin (7C2C3), RRID AB_2819193; Mouse monoclonal anti-occludin (OC-3F10), 33-1500, ThermoFisher, RRID AB_2533101; Rat monoclonal anti-ZO-1 (R40.76), RRID AB_2783859; Rabbit monoclonal anti-E-cadherin, 3195, Cell Signaling Technology, RRID AB_2291471; Mouse monoclonal anti-E-cadherin, 76055, Abcam, RRID AB_1310159; Rabbit polyclonal anti-CK2α, ab10466, Abcam, RRID AB_297210; Mouse monoclonal anti-β-actin, A1978, Sigma, RRID AB_476692; Rabbit monoclonal anti-CD3 (SP7), ab16669, Abcam, RRID AB_44342. IRDye 800CW goat anti-rabbit IgG, 925-32211, LI-COR Biosciences, RRID AB_2651127; IRDye 680LT goat anti-rabbit IgG, 926-68021, LI-COR Biosciences, RRID AB_ 10706309;

IRDye 680RD-goat anti-Mouse IgG, 925-68070, LI-COR Biosciences, RRID: AB_2651128; IRDye 800CW-goat anti-Mouse IgG, 926-32210, LI-COR Biosciences, RRID AB_621842; HRP-goat anti-rabbit IgG, 7074, Cell Signaling Technology, RRID AB_2099233; HRP-horse anti-mouse IgG, 7076, Cell Signaling Technology RRID AB_330924; Alexa 594 donkey anti-rabbit IgG highly cross-adsorbed F(ab')2 fragments, 711-586-152, Jackson ImmunoResearch, RRID AB_2340622; Alexa 488-donkey anti-mouse IgG highly cross-adsorbed F(ab')2 fragments, 715-546-151, Jackson ImmunoResearch RRID AB_2340850; and Alexa 488-donkey anti-rat IgG highly cross-adsorbed F(ab')2 fragments, 712-546-153, Jackson ImmunoResearch RRID AB_2340686 were used.

Epithelial Cell Isolation and Western Blot

Colonic epithelial cells were isolated as described (74, 75). Cell lysates were separated by SDS-PAGE, transferred to PVDF membranes, and incubated with primary antibodies. Secondary antibodies were conjugated to horseradish peroxidase or infrared dyes, and proteins were detected using HyBlotCL film or an Odyssex Fc imager (LI-COR), respectively. Quantification used ImageJ and ImageStudio software.

Histological and Immunofluorescence Staining and Microscopy

Colon segments were snap-frozen or formalin-fixed and paraffin-embedded (FFPE) as described (29, 34). H&E and picrosirius red (76) stains were performed on 5 μm paraffin sections. Sections (5 μm) of snap-frozen tissue were fixed in 1%PFA before permeabilization, blocking, and staining, as described (34, 75). Sections (5 μm) of paraffin-embedded tissue microarrays were deparaffinized, epitopes unmasked, and autofluorescence quenched as described (34).

H&E- and picrosirius red-stained tissues were imaged using a DMLB microscope (Leica) with 10× HC FL PLAN NA0.25, 20× HC FL PLAN FLUOTAR NA0.5, and 40× HC FL PLAN NA0.65 objectives and a MicroPublisher 3.3 CCD camera (QImaging) controlled by QCapture Pro 7.

Fluorescent micrographs were collected as stacks at 0.2 μm intervals using an Axioplan 2 (Zeiss) with Chroma single channel ET filter sets, 20× Plan-Apochromat NA0.8 or 63× Plan-Apochromat NA 1.4 immersion objective, and a Coolsnap HQ camera controlled by MetaMorph 7.8 (Molecular Devices). Images were deconvoluted using Autoquant X3 (MediaCybernetics).

Histopathological Scoring

Histopathological analysis of colitis was performed by a pathologist blinded to the experimental conditions. Colon tissues were scored on a scale of 0-3 for eight parameters, yielding a maximum score of 24. Scoring parameters were goblet cell depletion, mucosal hyperplasia, crypt cell apoptosis, epithelial erosion, lymphocytic infiltrate, polymorphonuclear (PMN) leukocyte infiltrate, crypt architectural distortion, and involvement of the submucosa. Fibrosis was scored on a 5 point scale on the basis of picrosirius red staining.

Quantification and Statistical Analysis

For all data shown, specific numbers of mice in each group are indicated in figure legends. Data are presented as mean ± SD. All data are representative of at least 3 independent experiments. Statistical significance was determined by two-tailed Student's t-test, ANOVA with Bonferroni's correction, 2-tailed Mann-Whitney U test, or Kaplan-Meier log-rank test, as indicated in the figure legends. Results with $P<0.05$ were considered significant. In figures, P values are indicated as * < 0.05, ** < 0.01, *** < 0.001.

Study Approval

All studies were approved by Institutional Animal Care and Use Committees at Brigham and Women's Hospital, Boston Children's Hospital, and The University of Chicago.

Author contributions

The project was conceived by JRT. PR, NS, PYT, PP, SCP, PRS, WTK, and JRT performed experiments. ST provided claudin-2 knockout mice. Figures were prepared by PR, NS, PP, and JRT. The manuscript was written by JRT and revised by PR and JRT with input from all authors.

Acknowledgments

This work was supported by Department of Defense Grant PR181271 (JRT), NIH grants R01DK61931 (JRT), R01DK68271 (JRT), and R24DK099803 (JRT), the Harvard Digestive Disease Center (P30DK034854), and Crohn's and Colitis Foundation Research Fellowship Award 622459 (NS). We thank Tiffany S. Davanzo (Slaybaugh Studios) for her beautiful illustrations, Heather Marlatt (Nationwide Histology) for her outstanding assistance with staining and tissue microarray development, and, alphabetically, Marion France (Brigham and Women's Hospital and Harvard Medical School), Ekaterina Khramtsova (The University of Chicago), Steven Nilsen (Brigham and Women's Hospital and Harvard Medical School), Lora M.D.M. Ong (Brigham and Women's Hospital and Harvard Medical School), Sheng-Ru Shiou (The University of Chicago), Christopher Weber (The University of Chicago), and Sunil Yeruva (Brigham and Women's Hospital and Harvard Medical School) for their assistance.

References

1. Tisher CC, and Yarger WE. Lanthanum permeability of the tight junction (zonula occludens) in the renal tubule of the rat. *Kidney Int.* 1973;3:238-50.
2. Marcial MA, Carlson SL, and Madara JL. Partitioning of paracellular conductance along the ileal crypt-villus axis: a hypothesis based on structural analysis with detailed consideration of tight junction structure-function relationships. *J Membr Biol.* 1984;80:59-70.
3. Pei L, Solis G, Nguyen MT, Kamat N, Magenheimer L, Zhuo M, Li J, Curry J, McDonough AA, Fields TA, et al. Paracellular epithelial sodium transport maximizes energy efficiency in the kidney. *J Clin Invest.* 2016;126:2509-18.
4. Wada M, Tamura A, Takahashi N, and Tsukita S. Loss of claudins 2 and 15 from mice causes defects in paracellular Na+ flow and nutrient transport in gut and leads to death from malnutrition. *Gastroenterol.* 2013;144:369-80.
5. Farquhar M, and Palade G. Junctional complexes in various epithelia. *J Cell Biol.* 1963;17:375-412.
6. Machen TE, Erlij D, and Wooding FB. Permeable junctional complexes. The movement of lanthanum across rabbit gallbladder and intestine. *J Cell Biol.* 1972;54:302-12.
7. Turner JR. Intestinal mucosal barrier function in health and disease. *Nat Rev Immunol.* 2009;9:799-809.
8. Anderson JM, and Van Itallie CM. Physiology and function of the tight junction. *Cold Spring Harb Perspect Biol.* 2009;1:a002584.
9. Shen L, Weber CR, Raleigh DR, Yu D, and Turner JR. Tight junction pore and leak pathways: a dynamic duo. *Annu Rev Physiol.* 2011;73:283-309.
10. Colegio OR, Van Itallie CM, McCrea HJ, Rahner C, and Anderson JM. Claudins create charge-selective channels in the paracellular pathway between epithelial cells. *Am J Physiol - Cell Physiol.* 2002;283:C142-7.
11. Rosenthal R, Milatz S, Krug SM, Oelrich B, Schulzke JD, Amasheh S, Gunzel D, and Fromm M. Claudin-2, a component of the tight junction, forms a paracellular water channel. *J Cell Sci.* 2010;123:1913-21.
12. Amasheh S, Meiri N, Gitter AH, Schoneberg T, Mankertz J, Schulzke JD, and Fromm M. Claudin-2 expression induces cation-selective channels in tight junctions of epithelial

cells. *J Cell Sci.* 2002;115:4969-76.

13. Rosenthal R, Gunzel D, Piontek J, Krug SM, Ayala-Torres C, Hempel C, Theune D, and Fromm M. Claudin-15 forms a water channel through the tight junction with distinct function compared to claudin-2. *Acta Physiol (Oxf).* 2020;228:e13334.
14. Weber CR, Liang GH, Wang Y, Das S, Shen L, Yu AS, Nelson DJ, and Turner JR. Claudin-2-dependent paracellular channels are dynamically gated. *eLife.* 2015;4:e09906.
15. Yu AS, Cheng MH, Angelow S, Gunzel D, Kanzawa SA, Schneeberger EE, Fromm M, and Coalson RD. Molecular basis for cation selectivity in claudin-2-based paracellular pores: identification of an electrostatic interaction site. *J Gen Physiol.* 2009;133:111-27.
16. Rosenthal R, Gunzel D, Krug SM, Schulzke JD, Fromm M, and Yu AS. Claudin-2-mediated cation and water transport share a common pore. *Acta Physiol (Oxf).* 2017;219:521-36.
17. Kiuchi-Saishin Y, Gotoh S, Furuse M, Takasuga A, Tano Y, and Tsukita S. Differential expression patterns of claudins, tight junction membrane proteins, in mouse nephron segments. *J Am Soc Nephrol.* 2002;13:875-86.
18. Escaffit F, Boudreau F, and Beaulieu JF. Differential expression of claudin-2 along the human intestine: Implication of GATA-4 in the maintenance of claudin-2 in differentiating cells. *J Cell Physiol.* 2005;203:15-26.
19. Aung PP, Mitani Y, Sanada Y, Nakayama H, Matsusaki K, and Yasui W. Differential expression of claudin-2 in normal human tissues and gastrointestinal carcinomas. *Virchows Arch.* 2006;448:428-34.
20. Uhlen M, Fagerberg L, Hallstrom BM, Lindskog C, Oksvold P, Mardinoglu A, Sivertsson A, Kampf C, Sjostedt E, Asplund A, et al. Proteomics. Tissue-based map of the human proteome. *Science.* 2015;347:1260419.
21. Muto S, Hata M, Taniguchi J, Tsuruoka S, Moriwaki K, Saitou M, Furuse K, Sasaki H, Fujimura A, Imai M, et al. Claudin-2-deficient mice are defective in the leaky and cation-selective paracellular permeability properties of renal proximal tubules. *Proc Natl Acad Sci USA.* 2010;107:8011-6.
22. Tamura A, Hayashi H, Imasato M, Yamazaki Y, Hagiwara A, Wada M, Noda T, Watanabe M, Suzuki Y, and Tsukita S. Loss of claudin-15, but not claudin-2, causes Na+ deficiency and glucose malabsorption in mouse small intestine. *Gastroenterol.*

2011;140:913-23.

23. Alberini G, Benfenati F, and Maragliano L. A refined model of claudin-15 tight junction paracellular architecture by molecular dynamics simulations. *PLoS One.* 2017;12:e0184190.
24. Tamura A, Kitano Y, Hata M, Katsuno T, Moriwaki K, Sasaki H, Hayashi H, Suzuki Y, Noda T, Furuse M, et al. Megaintestine in claudin-15-deficient mice. *Gastroenterol.* 2008;134:523-34.
25. Holmes JL, Van Itallie CM, Rasmussen JE, and Anderson JM. Claudin profiling in the mouse during postnatal intestinal development and along the gastrointestinal tract reveals complex expression patterns. *Gene Expr Patterns.* 2006;6:581-8.
26. Ong M, Yeruva S, Sailer A, Nilsen SP, and Turner JR. Differential regulation of claudin-2 and claudin-15 expression in children and adults with malabsorptive disease. *Lab Invest.* 2020;100:483-90.
27. Luettig J, Rosenthal R, Barmeyer C, and Schulzke JD. Claudin-2 as a mediator of leaky gut barrier during intestinal inflammation. *Tissue Barriers.* 2015;3:e977176.
28. Schumann M, Kamel S, Pahlitzsch ML, Lebenheim L, May C, Krauss M, Hummel M, Daum S, Fromm M, and Schulzke JD. Defective tight junctions in refractory celiac disease. *Ann N Y Acad Sci.* 2012;1258:43-51.
29. Tsai PY, Zhang B, He WQ, Zha JM, Odenwald MA, Singh G, Tamura A, Shen L, Sailer A, Yeruva S, et al. IL-22 Upregulates Epithelial Claudin-2 to Drive Diarrhea and Enteric Pathogen Clearance. *Cell Host Microbe.* 2017;21:671-81 e4.
30. Heller F, Florian P, Bojarski C, Richter J, Christ M, Hillenbrand B, Mankertz J, Gitter AH, Burgel N, Fromm M, et al. Interleukin-13 is the key effector Th2 cytokine in ulcerative colitis that affects epithelial tight junctions, apoptosis, and cell restitution. *Gastroenterol.* 2005;129:550-64.
31. Prasad S, Mingrino R, Kaukinen K, Hayes KL, Powell RM, MacDonald TT, and Collins JE. Inflammatory processes have differential effects on claudins 2, 3 and 4 in colonic epithelial cells. *Lab Invest.* 2005;85:1139-62.
32. Weber CR, Nalle SC, Tretiakova M, Rubin DT, and Turner JR. Claudin-1 and claudin-2 expression is elevated in inflammatory bowel disease and may contribute to early neoplastic transformation. *Lab Invest.* 2008;88:1110-20.

33. Graham WV, He W, Marchiando AM, Zha J, Singh G, Li HS, Biswas A, Ong M, Jiang ZH, Choi W, et al. Intracellular MLCK1 diversion reverses barrier loss to restore mucosal homeostasis. *Nat Med.* 2019;25:690-700.
34. Nalle SC, Zuo L, Ong M, Singh G, Worthylake AM, Choi W, Manresa MC, Southworth AP, Edelblum KL, Baker GJ, et al. Graft-versus-host disease propagation depends on increased intestinal epithelial tight junction permeability. *J Clin Invest.* 2019;129:902-14.
35. Su L, Nalle SC, Shen L, Turner ES, Singh G, Breskin LA, Khramtsova EA, Khramtsova G, Tsai PY, Fu YX, et al. TNFR2 activates MLCK-dependent tight junction dysregulation to cause apoptosis-mediated barrier loss and experimental colitis. *Gastroenterol.* 2013;145:407-15.
36. Suzuki M, Nagaishi T, Yamazaki M, Onizawa M, Watabe T, Sakamaki Y, Ichinose S, Totsuka M, Oshima S, Okamoto R, et al. Myosin light chain kinase expression induced via tumor necrosis factor receptor 2 signaling in the epithelial cells regulates the development of colitis-associated carcinogenesis. *PLoS One.* 2014;9:e88369.
37. Yi Z, Fan H, Liu X, Tang Q, Zuo D, and Yang J. Adrenomedullin improves intestinal epithelial barrier function by downregulating myosin light chain phosphorylation in ulcerative colitis rats. *Mol Med Rep.* 2015;12:3615-20.
38. Laukoetter MG, Nava P, Lee WY, Severson EA, Capaldo CT, Babbin BA, Williams IR, Koval M, Peatman E, Campbell JA, et al. JAM-A regulates permeability and inflammation in the intestine in vivo. *J Exp Med.* 2007;204:3067-76.
39. Vetrano S, Rescigno M, Cera MR, Correale C, Rumio C, Doni A, Fantini M, Sturm A, Borroni E, Repici A, et al. Unique role of junctional adhesion molecule-a in maintaining mucosal homeostasis in inflammatory bowel disease. *Gastroenterol.* 2008;135:173-84.
40. Bird L. T cells: IL-9 breaks down barriers. *Nat Rev Immunol.* 2014.
41. Ahmad R, Chaturvedi R, Olivares-Villagomez D, Habib T, Asim M, Shivesh P, Polk DB, Wilson KT, Washington MK, Van Kaer L, et al. Targeted colonic claudin-2 expression renders resistance to epithelial injury, induces immune suppression, and protects from colitis. *Mucosal Immunol.* 2014;7:1340-53.
42. Nishida M, Yoshida M, Nishiumi S, Furuse M, and Azuma T. Claudin-2 regulates colorectal inflammation via myosin light chain kinase-dependent signaling. *Dig Dis Sci.* 2013;58:1546-59.

43. Weber CR, Raleigh DR, Su L, Shen L, Sullivan EA, Wang Y, and Turner JR. Epithelial myosin light chain kinase activation induces mucosal interleukin-13 expression to alter tight junction ion selectivity. *J Biol Chem.* 2010;285:12037-46.
44. Gunzel D, and Yu AS. Claudins and the modulation of tight junction permeability. *Physiol Rev.* 2013;93:525-69.
45. Li J, Angelow S, Linge A, Zhuo M, and Yu AS. Claudin-2 pore function requires an intramolecular disulfide bond between two conserved extracellular cysteines. *Am J Physiol - Cell Physiol.* 2013;305:C190-6.
46. Van Itallie CM, Holmes J, Bridges A, Gookin JL, Coccaro MR, Proctor W, Colegio OR, and Anderson JM. The density of small tight junction pores varies among cell types and is increased by expression of claudin-2. *J Cell Sci.* 2008;121:298-305.
47. Angelow S, and Yu AS. Structure-function studies of claudin extracellular domains by cysteine-scanning mutagenesis. *J Biol Chem.* 2009;284:29205-17.
48. Van Itallie CM, Fanning AS, and Anderson JM. Reversal of charge selectivity in cation or anion-selective epithelial lines by expression of different claudins. *Am J Physiol - Renal Physiol.* 2003;285:F1078-84.
49. Hou J, Rajagopal M, and Yu AS. Claudins and the kidney. *Annu Rev Physiol.* 2013;75:479-501.
50. Raleigh DR, Boe DM, Yu D, Weber CR, Marchiando AM, Bradford EM, Wang Y, Wu L, Schneeberger EE, Shen L, et al. Occludin S408 phosphorylation regulates tight junction protein interactions and barrier function. *J Cell Biol.* 2011;193:565-82.
51. Leach MW, Bean AG, Mauze S, Coffman RL, and Powrie F. Inflammatory bowel disease in C.B-17 scid mice reconstituted with the CD45RBhigh subset of CD4+ T cells. *Am J Pathol.* 1996;148:1503-15.
52. Krug SM, Gunzel D, Conrad MP, Lee IF, Amasheh S, Fromm M, and Yu AS. Charge-selective claudin channels. *Ann N Y Acad Sci.* 2012;1257:20-8.
53. Cordenonsi M, Turco F, D'Atri F, Hammar E, Martinucci G, Meggio F, and Citi S. Xenopus laevis occludin. Identification of in vitro phosphorylation sites by protein kinase CK2 and association with cingulin. *Eur J Biochem.* 1999;264:374-84.
54. Dorfel MJ, Westphal JK, Bellmann C, Krug SM, Cording J, Mittag S, Tauber R, Fromm M, Blasig IE, and Huber O. CK2-dependent phosphorylation of occludin regulates the

interaction with ZO-proteins and tight junction integrity. *Cell communication and signaling : CCS.* 2013;11:40.

55. Koch S, Capaldo CT, Hilgarth RS, Fournier B, Parkos CA, and Nusrat A. Protein kinase CK2 is a critical regulator of epithelial homeostasis in chronic intestinal inflammation. *Mucosal Immunol.* 2013;6:136-45.
56. Borad MJ, Hubbard JM, Oh D-Y, Rha SY, Mody K, Lim JKC, and Richards DA. A phase IB study of CX-4945 in combination with gemcitabine plus cisplatin in the frontline systemic treatment of patients with advanced cholangiocarcinoma. *J Clin Oncol.* 2017;35:294-.
57. Marschke RF, Borad MJ, McFarland RW, Alvarez RH, Lim JK, Padgett CS, Von Hoff DD, O'Brien SE, and Northfelt DW. Findings from the phase I clinical trials of CX-4945, an orally available inhibitor of CK2. *J Clin Oncol.* 2011;29.
58. Martins LR, Lucio P, Melao A, Antunes I, Cardoso BA, Stansfield R, Bertilaccio MT, Ghia P, Drygin D, Silva MG, et al. Activity of the clinical-stage CK2-specific inhibitor CX-4945 against chronic lymphocytic leukemia. *Leukemia.* 2014;28:179-82.
59. Jung M, Park KH, Kim HM, Kim TS, Zhang X, Park SM, Beom SH, Kim HS, Cheong JH, Chung HC, et al. Inhibiting casein kinase 2 overcomes paclitaxel resistance in gastric cancer. *Gastric Cancer.* 2019;22:1153-63.
60. Sharma D, Malik A, Guy CS, Karki R, Vogel P, and Kanneganti TD. Pyrin Inflammasome Regulates Tight Junction Integrity to Restrict Colitis and Tumorigenesis. *Gastroenterol.* 2018;154:948-64 e8.
61. el Marjou F, Janssen KP, Chang BH, Li M, Hindie V, Chan L, Louvard D, Chambon P, Metzger D, and Robine S. Tissue-specific and inducible Cre-mediated recombination in the gut epithelium. *Genesis.* 2004;39:186-93.
62. Shen L, and Turner JR. Actin depolymerization disrupts tight junctions via caveolae-mediated endocytosis. *Mol Biol Cell.* 2005;16:3919-36.
63. Shen L, Weber CR, and Turner JR. The tight junction protein complex undergoes rapid and continuous molecular remodeling at steady state. *J Cell Biol.* 2008;181:683-95.
64. Haljamae H, Jodal M, and Lundgren O. Countercurrent multiplication of sodium in intestinal villi during absorption of sodium chloride. *Acta Physiol Scand.* 1973;89:580-93.

65. Kleinewietfeld M, Manzel A, Titze J, Kvakan H, Yosef N, Linker RA, Muller DN, and Hafler DA. Sodium chloride drives autoimmune disease by the induction of pathogenic TH17 cells. *Nature.* 2013;496:518-22.

66. Wu C, Yosef N, Thalhamer T, Zhu C, Xiao S, Kishi Y, Regev A, and Kuchroo VK. Induction of pathogenic TH17 cells by inducible salt-sensing kinase SGK1. *Nature.* 2013;496:513-7.

67. Hernandez AL, Kitz A, Wu C, Lowther DE, Rodriguez DM, Vudattu N, Deng S, Herold KC, Kuchroo VK, Kleinewietfeld M, et al. Sodium chloride inhibits the suppressive function of FOXP3+ regulatory T cells. *J Clin Invest.* 2015;125:4212-22.

68. Aguiar SLF, Miranda MCG, Guimaraes MAF, Santiago HC, Queiroz CP, Cunha PDS, Cara DC, Foureaux G, Ferreira AJ, Cardoso VN, et al. High-Salt Diet Induces IL-17-Dependent Gut Inflammation and Exacerbates Colitis in Mice. *Frontiers in immunology.* 2017;8:1969.

69. Guo HX, Ye N, Yan P, Qiu MY, Zhang J, Shen ZG, He HY, Tian ZQ, Li HL, and Li JT. Sodium chloride exacerbates dextran sulfate sodium-induced colitis by tuning proinflammatory and antiinflammatory lamina propria mononuclear cells through p38/MAPK pathway in mice. *World J Gastroenterol.* 2018;24:1779-94.

70. Siddiqui-Jain A, Drygin D, Streiner N, Chua P, Pierre F, O'Brien SE, Bliesath J, Omori M, Huser N, Ho C, et al. CX-4945, an orally bioavailable selective inhibitor of protein kinase CK2, inhibits prosurvival and angiogenic signaling and exhibits antitumor efficacy. *Cancer Res.* 2010;70:10288-98.

71. Ferguson AD, Sheth PR, Basso AD, Paliwal S, Gray K, Fischmann TO, and Le HV. Structural basis of CX-4945 binding to human protein kinase CK2. *FEBS Lett.* 2011;585:104-10.

72. Pinto D, Robine S, Jaisser F, El Marjou FE, and Louvard D. Regulatory sequences of the mouse villin gene that efficiently drive transgenic expression in immature and differentiated epithelial cells of small and large intestines. *J Biol Chem.* 1999;274:6476-82.

73. France M, Skorich E, Kadrofske M, Swain GM, and Galligan JJ. Sex-related differences in small intestinal transit and serotonin dynamics in high-fat-diet-induced obesity in mice. *Exp Physiol.* 2016;101:81-99.

74. Nik AM, and Carlsson P. Separation of intact intestinal epithelium from mesenchyme. *BioTechniques.* 2013;55:42-4.

75. Clayburgh DR, Barrett TA, Tang Y, Meddings JB, Van Eldik LJ, Watterson DM, Clarke LL, Mrsny RJ, and Turner JR. Epithelial myosin light chain kinase-dependent barrier dysfunction mediates T cell activation-induced diarrhea in vivo. *J Clin Invest.* 2005;115:2702-15.

76. Junqueira LC, Bignolas G, and Brentani RR. Picrosirius staining plus polarization microscopy, a specific method for collagen detection in tissue sections. *Histochem J.* 1979;11:447-55.

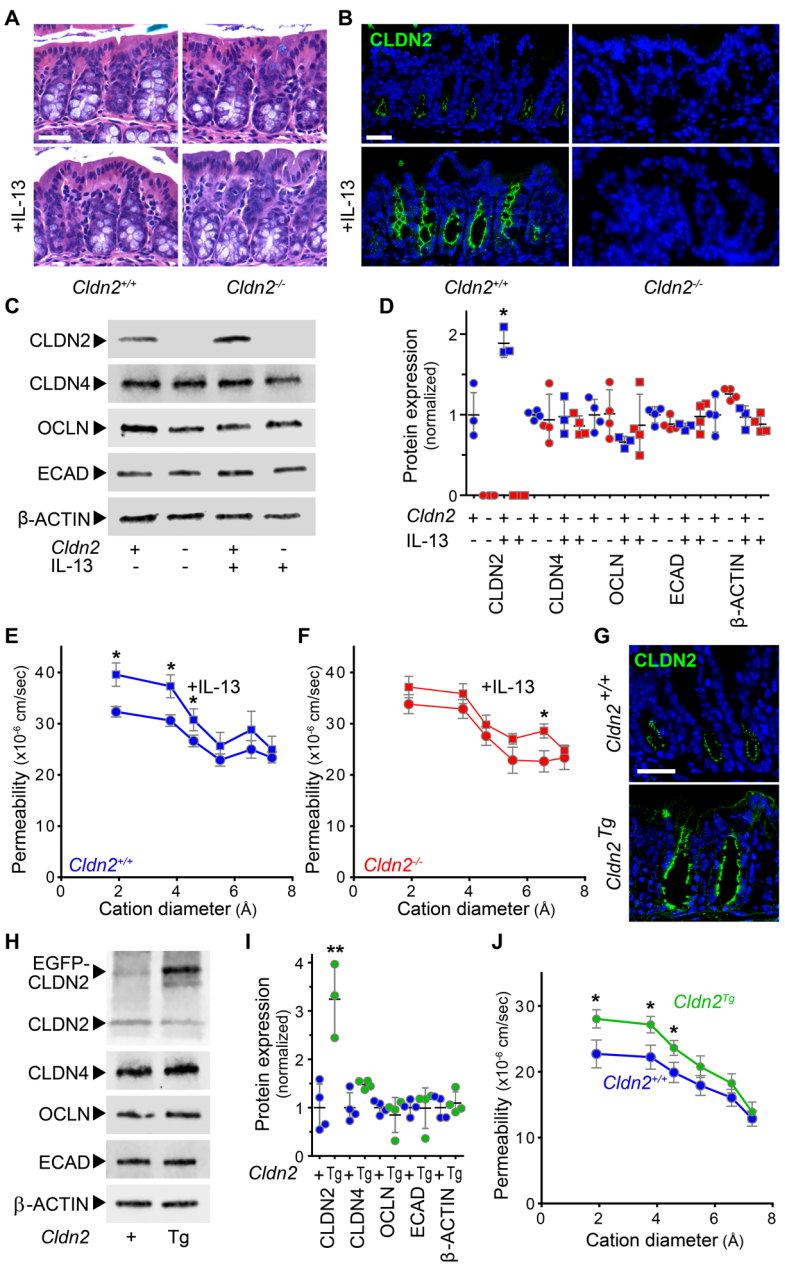

Figure 1. Claudin-2 is necessary and sufficient for IL-13 induced changes in pore pathway permeability. **(A)** Colonic histopathology of *Cldn2*$^{+/+}$ or *Cldn2*$^{-/-}$ mice is not affected by injection with vehicle or IL-13 (+IL-13). Bar = 50 μm. **(B)** IL-13 increases claudin-2 (CLDN2, green) protein expression in proximal colonic epithelial cells of *Cldn2*$^{+/+}$, but not *Cldn2*$^{-/-}$, mice. Nuclei (blue) are shown for reference. Bar = 50 μm. **(C)** Immunoblots of isolated colonic epithelia from *Cldn2*$^{+/+}$ and *Cldn2*$^{-/-}$ mice treated with vehicle or IL-13. Claudin-2 (CLDN2), claudin-4 (CLDN4), occludin (OCLN), E-cadherin (ECAD), and β-actin (β-ACTIN) are shown. **(D)** Densitometry of immunoblots, as in C. *n* = 3-4 per condition. ANOVA with Bonferroni's correction. **(E, F)** Proximal colonic mucosae from *Cldn2*$^{+/+}$ (E) and *Cldn2*$^{-/-}$ (F) mice treated with vehicle (circles) or IL-13 (+IL-13, squares) were mounted in Ussing chambers for analysis of paracellular permeability. Bi-ionic potential measurements were used to determine the permeabilities of Na^+ and five larger cations (methylamine, ethylamine, tetramethylammonium, tetraethylammonium, and N-methyl-D-glucamine). IL-13 increased permeability of Na^+ and methylamine, but not larger cations, in *Cldn2*$^{+/+}$ mice. IL-13 did not affect Na^+ or methylamine permeability in *Cldn2*$^{-/-}$ mice. *n* = 8 and 9 for *Cldn2*$^{+/+}$ mice without or with IL-13 treatment, respectively, and *n* = 5 and 9 for *Cldn2*$^{-/-}$ mice without or with IL-13 treatment, respectively. Data are compiled from three independent experiments. 2-tailed t-test. **(G)** Claudin-2 (CLDN2, green) expression in *Cldn2*$^{+/+}$ and *Cldn2*^{Tg} mice. Bar = 50 μm. **(H)** Representative immunoblots of isolated colonic epithelia from *Cldn2*$^{+/+}$ and *Cldn2*^{Tg} mice. **(I)** Densitometry of immunoblots *Cldn2*$^{+/+}$ (blue circles) and *Cldn2*^{Tg} (green circles) mice, as in H. *n* = 3-4 per condition. 2-tailed t-test. **(J)** Ussing chamber analysis (as in E) of proximal colonic mucosae from *Cldn2*$^{+/+}$ and *Cldn2*^{Tg} mice. Claudin-2 overexpression selectively increased Na^+ and methylamine permeability. *n* = 11 *Cldn2*$^{+/+}$, 10 *Cldn2*^{Tg}. Data are a compiled from three independent experiments. 2-tailed t-test. *, $P < 0.05$; **, $P < 0.01$.

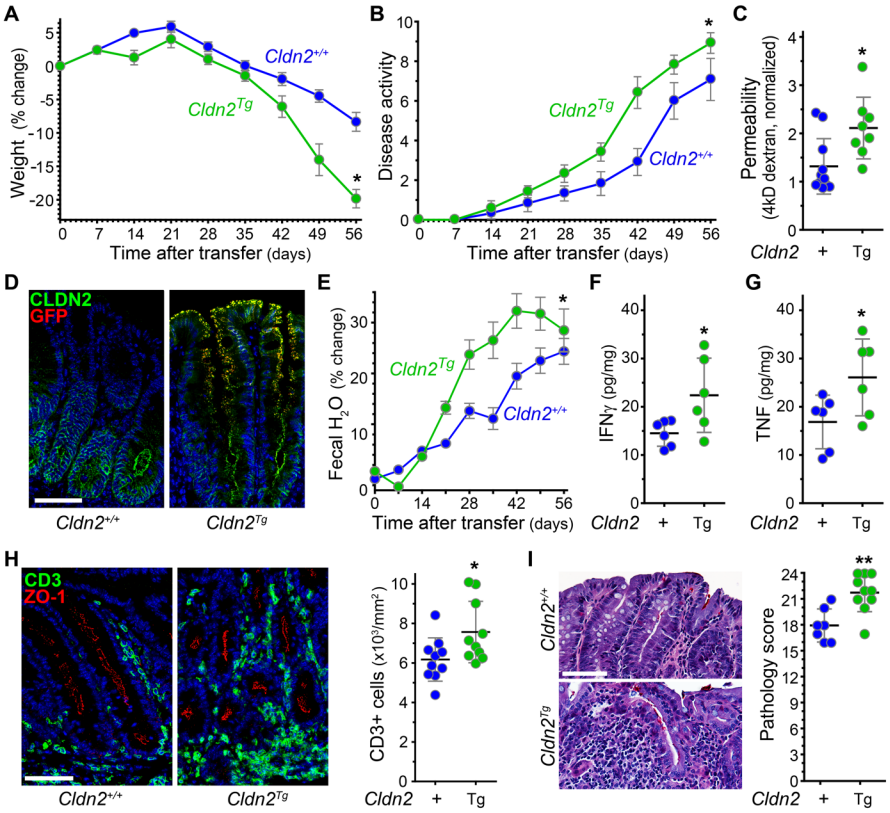

Figure 2. Intestinal epithelial-specific claudin-2 overexpression exacerbates immune-mediated colitis. (A) Weight loss and **(B)** disease activity following T cell transfer were both greater in *Cldn2*^{Tg} *Rag1*$^{-/-}$ mice (*Cldn2*^{Tg}, green circles) relative to *Cldn2*$^{+/+}$ *Rag1*$^{-/-}$ mice (*Cldn2*$^{+/+}$, blue circles) *n* = 12 per genotype. 2-tailed t-test at day 56. **(C)** Consistent with greater tissue injury, increases in 4kD dextran permeability were amplified in *Cldn2*^{Tg} *Rag1*$^{-/-}$ mice relative to *Cldn2*$^{+/+}$ *Rag1*$^{-/-}$ mice. *n* = 12 per genotype. 2-tailed t-test. **(D)** Claudin-2 expression per cell as well as the number of claudin-2 positive cells in each crypt increased markedly at day 56. Endogenous claudin-2 (CLDN2, green) was limited to the bottom half of the crypt in both *Cldn2*$^{+/+}$ *Rag1*$^{-/-}$ and *Cldn2*^{Tg} *Rag1*$^{-/-}$ mice. In contrast, EGFP-claudin-2 (red) was detected from the mid crypt to the mucosal surface. Bar = 50 μm. **(E)** Fecal water of *Cldn2*$^{+/+}$ *Rag1*$^{-/-}$ and *Cldn2*^{Tg} *Rag1*$^{-/-}$ mice following T cell transfer. *n* = 12 per genotype. 2-tailed t-test. **(F)** Mucosal IFNγ and **(G)** TNF on day 56. *n* = 6 per genotype. 2-tailed t-test. **(H)** Representative immunostain of proximal colon showing CD3 (green) and ZO-1 (red) and corresponding quantitative analysis. Bar = 50 μm. *n* = 10 per genotype. 2-tailed t-test. **(I)** Representative histopathology and pathology scores at day 56. Bar = 50 μm. *n* = 7 *Cldn2*$^{+/+}$ *Rag1*$^{-/-}$, 10 *Cldn2*^{Tg} *Rag1*$^{-/-}$. 2-tailed t-test. Data presented in this figure are typical of three independent experiments. *, *P*< 0.05; **, *P*< 0.01.

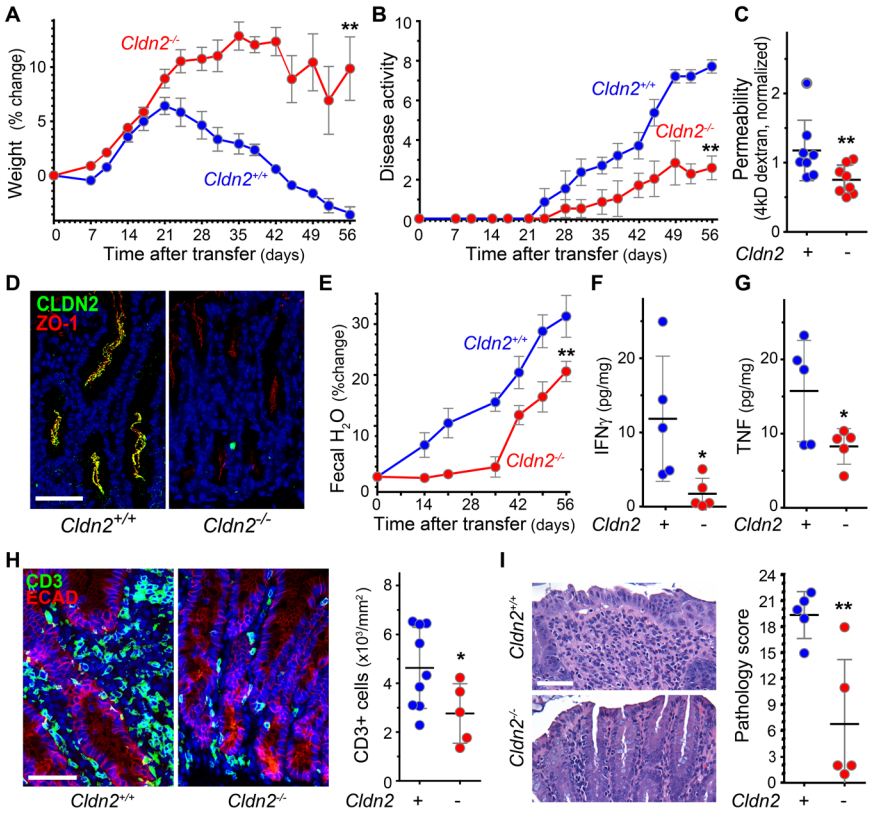

Figure 3. Claudin-2 knockout limits immune-mediated colitis severity. (A) Weight loss and **(B)** disease activity induced by T cell transfer are attenuated in *Cldn2*$^{-/-}$ *Rag1*$^{-/-}$ mice (*Cldn2*$^{-/-}$, red circles), relative to of *Cldn2*$^{+/+}$ *Rag1*$^{-/-}$ mice (*Cldn2*$^{+/+}$, blue circles). *n* = 9-10 per genotype. 2-tailed t-test at day 56. **(C)** Consistent with reduced mucosal damage, barrier function was maintained in *Cldn2*$^{-/-}$ *Rag1*$^{-/-}$ mice relative to of *Cldn2*$^{+/+}$ *Rag1*$^{-/-}$ mice. 4kD dextran flux was normalized to mice without T cell transfer. *n* = 8 per genotype. 2-tailed t-test. **(D)** Claudin-2 (CLDN2, green) expression is increased in proximal colon of *Cldn2*$^{+/+}$ *Rag1*$^{-/-}$ mice at day 56. ZO-1 (red) expression is maintained in *Cldn2*$^{+/+}$ *Rag1*$^{-/-}$ and *Cldn2*$^{-/-}$ *Rag1*$^{-/-}$ mice. Bar = 50 μm. **(E)** Following T cell transfer, fecal water content increased more rapidly in *Cldn2*$^{+/+}$ *Rag1*$^{-/-}$ mice relative to *Cldn2*$^{-/-}$ *Rag1*$^{-/-}$ mice. *n* = 5 per genotype. 2-tailed t-test at day 56. **(F)** Mucosal IFNγ and **(G)** TNF on day 56 after T cell transfer. *n* = 5 per genotype. 2-tailed t-test. **(H)** Representative immunostain of proximal colon showing CD3 (green) and E-cadherin (ECAD, red) and corresponding quantitative analysis. T cell recruitment is blunted in *Cldn2*$^{-/-}$ *Rag1*$^{-/-}$ mice. Bar = 50 μm. *n* = 5-9 per genotype. 2-tailed t-test. **(I)** Representative histopathology and pathology scores at day 56. Bar = 50 μm. *n* = 5 per genotype. 2-tailed t-test. Data presented in this figure are typical of five independent experiments. *, *P*< 0.05; **, *P*< 0.01.

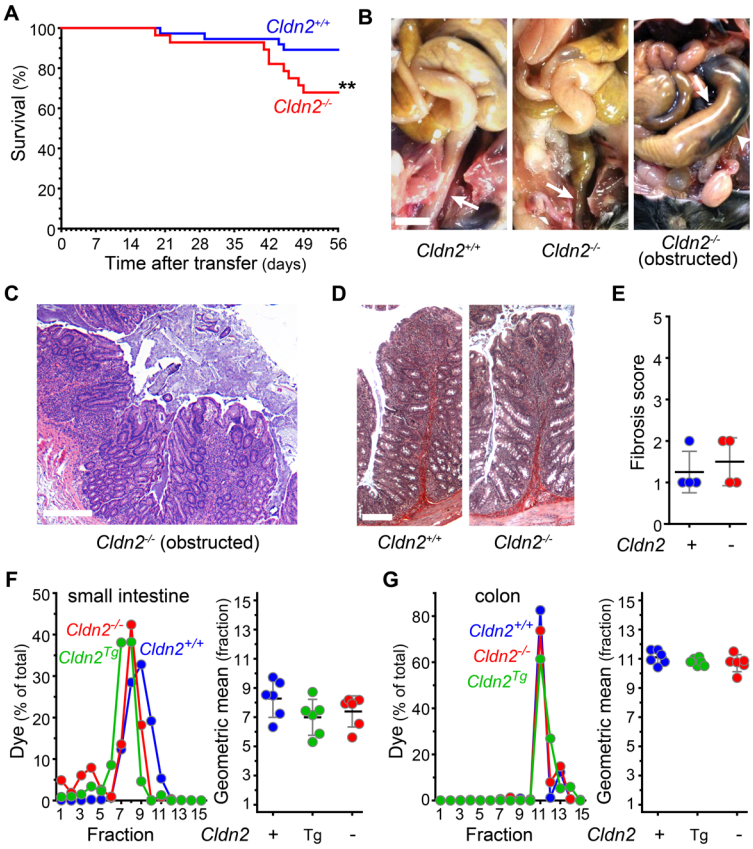

Figure 4. Despite reduced immune-mediated colitis severity, survival is compromised in claudin-2 knockout mice. (A) Survival of *Cldn2*$^{+/+}$ *Rag1*$^{-/-}$ (*Cldn2*$^{+/+}$, blue line) and *Cldn2*$^{-/-}$ *Rag1*$^{-/-}$ (*Cldn2*$^{-/-}$, red line) mice following T cell transfer. *n* = 14-17 per genotype. Kaplan-Meier log-rank test. Data are representative of five independent experiments **(B)** Representative gross images of non-obstructed colons (arrows) of *Cldn2*$^{+/+}$ and *Cldn2*$^{-/-}$ mice, and obstructed (arrow) and ischemic (arrowhead) colon of *Cldn2*$^{-/-}$ mice. Bar = 0.5 cm. **(C)** Representative histopathology of obstructed *Cldn2*$^{-/-}$ mouse colon. Bar = 50 µm. **(D)** Picrosirius red stains of *Cldn2*$^{+/+}$ and *Cldn2*$^{-/-}$ mice colon at day 56. Bar = 50 µm. **(E)** Fibrosis scores of colons from *Cldn2*$^{+/+}$ (blue circles) and *Cldn2*$^{-/-}$ (red circles) mice at day 56. *n* = 4 per genotype. 2-tailed t-test. **(F)** Small intestine motility in *Cldn2*$^{+/+}$, *Cldn2*^{Tg} (green circles), and *Cldn2*$^{+/+}$ mice assessed as dye content of each fraction and geometric mean of dye distribution. *n* = 6 per genotype. ANOVA with Bonferroni's correction. **(G)** Colonic motility assessed as dye content of each fraction and geometric mean of dye distribution. *n* = 6 per genotype. ANOVA with Bonferroni's correction. **, $P < 0.01$.

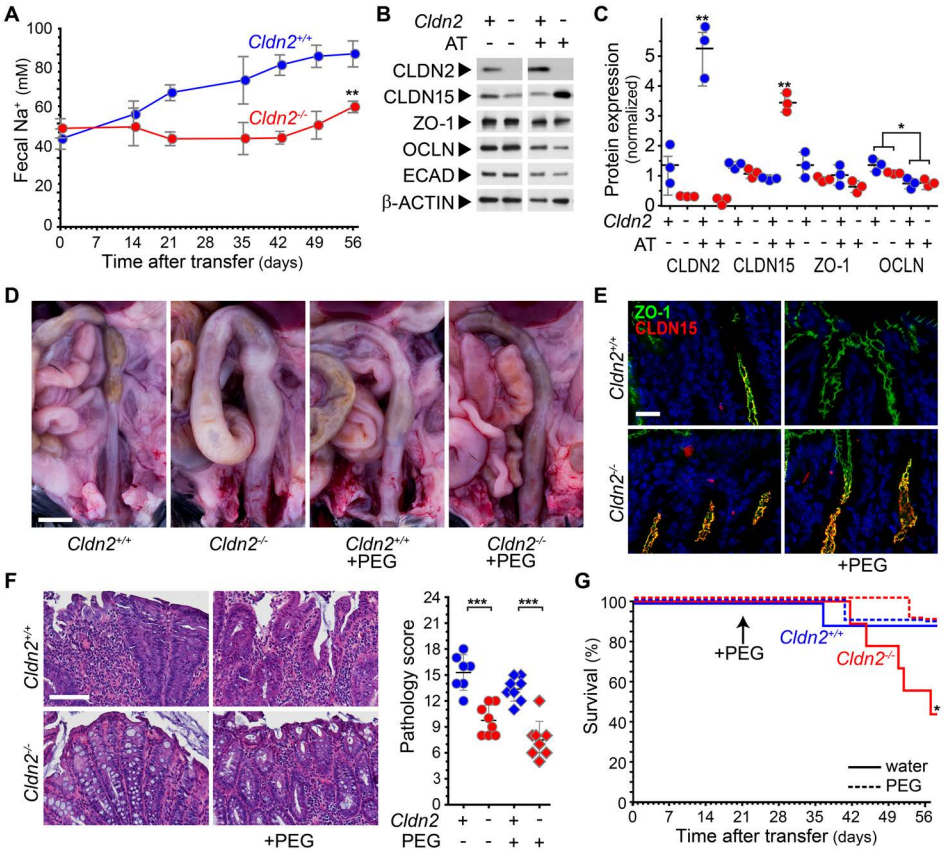

Figure 5. Insufficient luminal hydration leads to increased mortality in claudin-2 knockout mice. (A) Fecal Na^+ of *Cldn2*$^{+/+}$ *Rag1*$^{-/-}$ (*Cldn2*$^{+/+}$, blue circles) and *Cldn2*$^{-/-}$ *Rag1*$^{-/-}$ (*Cldn2*$^{-/-}$, red circles) mice following T cell transfer. Data are representative of five independent experiments. *n* = 6 per genotype. 2-tailed t-test at day 56. **(B)** Immunoblots of isolated colonic epithelia from *Cldn2*$^{+/+}$ *Rag1*$^{-/-}$ and *Cldn2*$^{-/-}$ *Rag1*$^{-/-}$ mice without (-) or with (+) T cell transfer (AT) at day 56. Claudin-2 (CLDN2), claudin-15 (CLDN15), ZO-1, occludin (OCLN), E-cadherin (ECAD), and β-actin (β-ACTIN) are shown. Due to the number of antigens probed, samples are not all from the same membrane but are from blots that were performed in parallel using the same samples. The data are validated further by the quantitative densitometry. **(C)** Densitometry of immunoblots, as in B. *n* = 3 per condition. ANOVA with Bonferroni's correction. Data are representative of three independent experiments. **(D)** Gross images of *Cldn2*$^{+/+}$ *Rag1*$^{-/-}$ and *Cldn2*$^{-/-}$ *Rag1*$^{-/-}$ mouse colons with (+PEG) or without polyethylene glycol treatment at day 56. Bar = 0.5 cm. **(E)** ZO-1 (green) and claudin-15 (CLDN15, red) expression in proximal colon of vehicle- and PEG-treated mice 56 days after T cell transfer. Bar = 20 μm. **(F)** Representative colonic histopathology and pathology scores in *Cldn2*$^{+/+}$ *Rag1*$^{-/-}$ and *Cldn2*$^{-/-}$ *Rag1*$^{-/-}$ mice without (circles) or with (+PEG, diamonds) polyethylene glycol treatment at day 56. Bar = 50 μm. *n* = 7-8 per genotype and condition. ANOVA with Bonferroni's correction. **(G)** Survival of *Cldn2*$^{+/+}$ *Rag1*$^{-/-}$ (blue lines) and *Cldn2*$^{-/-}$ *Rag1*$^{-/-}$ (red lines) mice following provision of normal drinking water (solid lines) or water with polyethylene glycol (+PEG, dashed lines) beginning at day 21. *n* = 9-10 per condition. Kaplan-Meier log-rank test. Data in D – G are representative of three independent experiments. *, $P < 0.05$; **, $P < 0.01$; ***, $P < 0.001$.

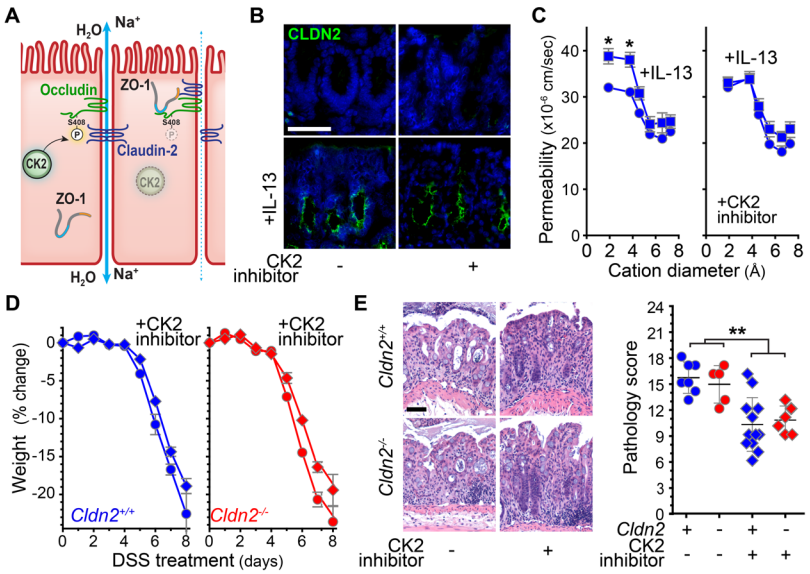

Figure 6. CK2 inhibition does not affect DSS colitis severity. (A) In vitro studies have shown that casein kinase-2 (CK2) inhibition results in occludin S408 dephosphorylation. This increases occludin affinity for ZO-1 and leads to assembly of a trimolecular complex composed of occludin, ZO-1, and claudin-2 that inactivates claudin-2 channels (50). **(B)** Claudin-2 (CLDN2, green) expression in proximal colon of wildtype mice treated with vehicle or IL-13 (+IL-13) without or with CK2 inhibition. Nuclei (blue) are shown for reference. Data are representative of three independent experiments. Bar = 50 μm. **(C)** Ussing chamber analysis of proximal colonic mucosal permeability to Na^+ and five larger cations (methylamine, ethylamine, tetramethylammonium, tetraethylammonium, and N-methyl-D-glucamine), as in Figure 1. Both graphs show *Cldn2*$^{+/+}$ mice treated with vehicle (circles) or IL-13 (+IL-13, squares). Mice that were treated with vehicle (left) or CK2 inhibitor (right) are shown in the two graphs. Data are compiled from three independent experiments. ANOVA with Bonferroni's correction. **(D)** Weight change of *Cldn2*$^{+/+}$ and *Cldn2*$^{-/-}$ mice following DSS treatment without (circles) or with (diamonds) CK2 inhibitor. *n* = 5-7 per group. ANOVA with Bonferroni's correction. **(E)** Representative histopathology and pathology scores at day 8 after DSS treatment. Bar = 50 μm. *n* = 5-12 per group. ANOVA with Bonferroni's correction. Data in D – F are representative of four independent experiments. *, *P*< 0.05; **, *P*< 0.01.

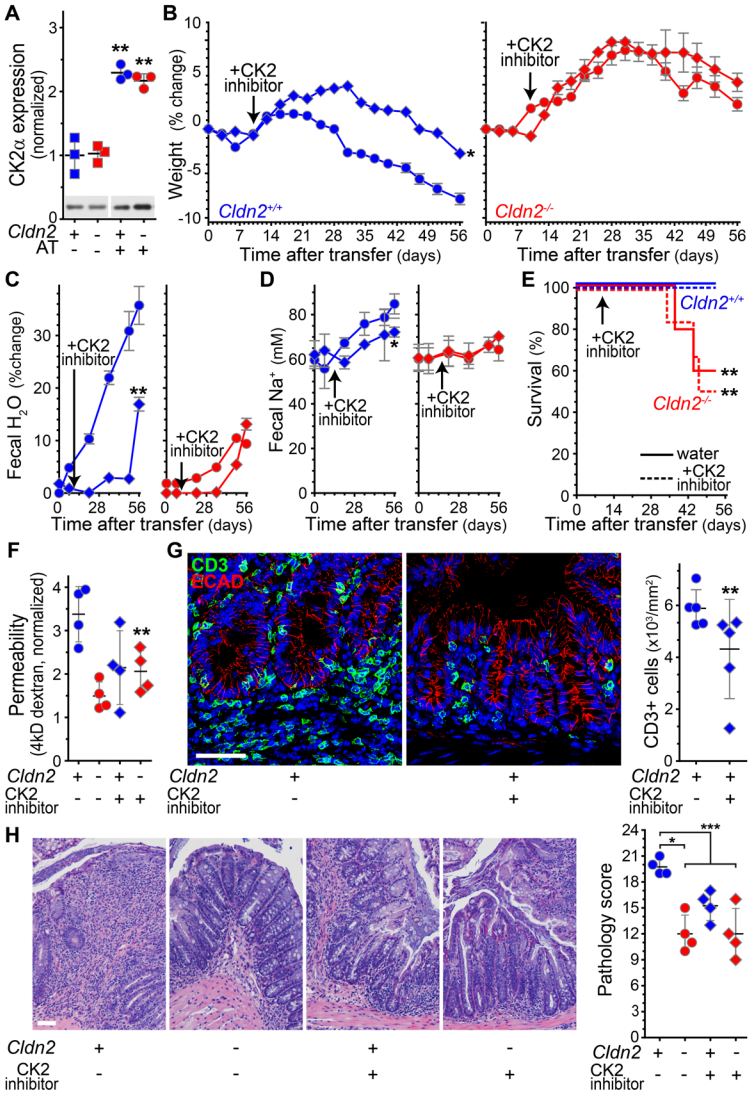

Figure 7. CK2 inhibition limits immune-mediated colitis severity via a claudin-2-dependent mechanism. **(A)** Immunoblots of casein kinase (CK2) in isolated colonic epithelia from *Cldn2*$^{+/+}$ *Rag1*$^{-/-}$ (*Cldn2*$^{+/+}$, blue symbols) and *Cldn2*$^{-/-}$ *Rag1*$^{-/-}$ (*Cldn2*$^{-/-}$, red symbols) mice at day 56 after adoptive T cell transfer (+AT). *n* = 3 per condition. Data are representative of three independent experiments. ANOVA with Bonferroni's correction. **(B)** Weight loss following T cell transfer was attenuated by CK2 inhibition in *Cldn2*$^{+/+}$ *Rag1*$^{-/-}$ mice but not *Cldn2*$^{-/-}$ *Rag1*$^{-/-}$ mice. Mice were treated with vehicle (circles) or CK2 inhibitor (diamonds), beginning 10 days after T cell transfer. *n* = 5-6 per condition. ANOVA with Bonferroni's correction at day 56. **(C)** Fecal water and **(D)** Na^+ content following T cell transfer were reduced in CK2 inhibitor-treated *Cldn2*$^{+/+}$ *Rag1*$^{-/-}$ mice; there was no effect in *Cldn2*$^{-/-}$ *Rag1*$^{-/-}$ mice. *n* = 5-6 per condition. ANOVA with Bonferroni's correction at day 56. **(E)** Survival of *Cldn2*$^{+/+}$ *Rag1*$^{-/-}$ and *Cldn2*$^{-/-}$ *Rag1*$^{-/-}$ mice following T cell transfer without (solid lines) or with (dashed lines) CK2 inhibitor treatment. *n* = 5-6 per condition. Kaplan-Meier log-rank test. **(F)** Intestinal barrier function at day 56 after T cell transfer was preserved in CK2 inhibitor-treated *Cldn2*$^{+/+}$ *Rag1*$^{-/-}$ mice. *n* = 4 per condition. ANOVA with Bonferroni's correction. **(G)** Immunostain of CD3 (green) and E-cadherin (ECAD, red). CK2 inhibition reduced T cell recruitment into proximal colonic mucosae of *Cldn2*$^{+/+}$ *Rag1*$^{-/-}$ mice. Bar = 50 μm. *n* = 5 per condition. ANOVA with Bonferroni's correction. **(H)** Histopathology and scores at day 56 after T cell transfer without or with CK2 inhibitor treatment. Bar = 50 μm. *n* = 4 per genotype and condition. Data presented in B – H are typical of three independent experiments. ANOVA with Bonferroni's correction. *, $P < 0.05$; **, $P < 0.01$; ***, $P < 0.001$.